Journal of Electronic Materials (2022) 51:3843–3850
https://doi.org/10.1007/s11664-022-09644-1

ORIGINAL RESEARCH ARTICLE

Gas-Sensing Properties and Preparation of Waste Mask Fibers/ZnS Composites

Q. Y. Wang[1,2] · Z. F. Wu[1,2] · M. Zhang[1,2] · Z. J. Qin[1,2] · L. Wang[1,2] · F. R. Zhong[3] · H. M. Duan[1,2]

Received: 22 December 2021 / Accepted: 5 April 2022 / Published online: 26 April 2022

Abstract

To realize the resource utilization of waste mask fibers (MF), a layer of ZnS nanoparticles was grown on MF by a one-step hydrothermal method, and a MF/ZnS sensor was successfully prepared. This is the first time that resource utilization of MF has been combined with the development of a high-performance gas sensor. The MF/ZnS sensor showed high sensitivity and recoverability to target vapors at room temperature. Compared with ZnS powder loaded on a ceramic substrate, the MF/ZnS composite responses to four analytes have been improved by 8.4~35.2 times. In addition, the time for the MF/ZnS sensor to complete one response–recovery cycle for all four analytes was less than 30 s. This should be attributed to the high gas permeability of the MF substrate, which made the ZnS particles loaded on the MF more fully exposed to contact with the target vapors. This work not only provides a simple and low-cost method to optimize the sensing performance of gas sensors but also provides a new way for the resource utilization of MF.

Graphic Abstract

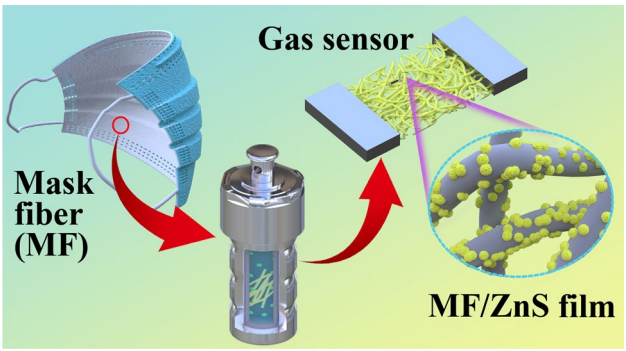

Keywords Waste mask · electronic materials · gas sensor · nanocomposites

✉ Z. F. Wu
wuzf@xju.edu.cn

✉ M. Zhang
minzhang0816@163.com

✉ H. M. Duan
dhm@xju.edu.cn

[1] Xinjiang Key Laboratory of Solid State Physics and Devices, Urumqi 830046, Xinjiang, China

[2] School of Physics Science and Technology, Xinjiang University, Urumqi 830046, Xinjiang, China

[3] School of Physics and Electronic Science, Zunyi Normal College, Zunyi 563006, Guizhou, People's Republic of China

Introduction

During the COVID-19 pandemic, disposable masks have prevented the spread of pathogens and protected us from the virus.[1] In this context, a large number of disposable masks are needed in every country and region of the world. The World Health Organization (WHO) estimates that 89 million masks are needed every month, requiring a 40% increase in production to fill the huge supply and demand gap during the pandemic.[2] At the same time, a large number of waste masks have been produced all over the world during the

pandemic. The main component of waste masks is polypropylene (PP) fibers, which take hundreds of years or more to degrade in the environment, slowly turning into microplastics.[3] Microplastics in soil and water can be absorbed by plants and plankton, and can be enriched in fish, animals, and humans, which will cause potential harm.[4] It is estimated that, by 2020, at least 1.56 billion surgical masks have been discharged into the ocean, posing a threat to marine creatures and ecosystems.[5] The traditional handling methods of waste mask fibers (MF), such as incineration and landfill, can also cause serious pollution to soil and water sources. Therefore, it is particularly urgent to find a new solution for resource utilization different from the traditional incineration and landfill treatment.[6,7] For example, Singh et al.[8] used a one-step preparation method to impregnate surface-modified silica particles on commercial PP nonwovens to produce superhydrophobic properties and excellent oil–water separation capabilities. Soochan et al.[9] sulfonated MFs soaked in fuming sulfuric acid to prepare a separator with high safety and excellent electrochemical properties for water-based rechargeable batteries. There are only a few studies on the recycling of used masks, which achieved good results. However, there is still relatively little research on the resource utilization of used masks compared to the large number of used masks waiting for disposal. Therefore, more research is needed to develop a new path for the resource utilization of waste masks.

On the other hand, gas sensors are one of the core devices of the Internet of Things and the Industrial Internet of Things, and play an increasing role in production and life.[10–13] With increasing attention on industrial safety, environmental pollution, air quality, accurate detection and early warning of flammable, and explosive and toxic gases have become the main challenges.[14–18] For example, hydrogen peroxide (H_2O_2) plays an important role in the food industry, textile industry, pharmaceutical research, and medical diagnosis.[19–25] However, if too much H_2O_2 enters the body through the respiratory tract, it can lead to genetic mutations and lung damage.[26] Therefore, there is a general trend to develop a high-performance gas sensor to monitor flammable, explosive, and toxic gases. Ideally, gas sensors should have high sensitivity, high selectivity, fast detection, low cost, and can work at low temperatures.[27,28] In the past few decades, although the gas-sensitive performance of metal oxide semiconductors has made many satisfactory results, the poor selectivity and the high working temperature (150~400°C) remain to be improved.[10,28] The stability and service life of sensors can be affected by the high working temperature. The high working temperature of a sensor can also pose ignition risks in the detection of flammable and explosive analytes.[15,29,30] What is more, ceramics, plastic, and rubber with low gas permeability are commonly used as sensing substrates in current gas sensors.[25,31] The low gas permeability of sensing substrates hinders the effective exposure of sensing materials to the target gas, limiting the improvement of the gas-sensing performance.[32,33] It is well known that disposable masks have excellent gas permeability. Moreover, due to their disposable use, the MFs of waste masks still maintain a good state and can be used as a sensing substrate.

As far as we know, the application of MFs in the field of gas sensors has not previously been reported. In this work, the resource utilization of MFs has been combined with the development of high-performance sensors to solve the above-mentioned problems. A layer of ZnS nanoparticles was successfully grown onto the MFs by a one-step hydrothermal method to prepare MF/ZnS sensors. The gas-sensing performance of a MF/ZnS sensor for H_2O_2 at room temperature was tested. At the same time, the influence of MFs with good gas permeability on the gas-sensing performance of MF/ZnS has been analyzed.

Materials and Methods

Materials

Used medical masks were produced by Xinjiang Jintianshan Medical Equipment, and were worn by students at Xinjiang University. Zinc acetate was purchased from Tianjin Shengao, and L-cysteine was purchased from Aladdin.

Synthesis

A MF/ZnS composite film was prepared by a one-step hydrothermal method[34] at 160°C for 6 h (Fig. 1). First, the MF was disinfected with medical alcohol and cut into strips. Second, the cleaned MF was added to the mixture of zinc acetate and L-cysteine for 20 min and then put into the drying box for hydrothermal reaction at 160°C for 6 h. Third, the MF/ZnS film was put into deionized water for ultrasonic treatment and dried at room temperature. After the sample was taken out, the remaining solution was centrifuged, and the precipitate of ZnS nanoparticles was collected and coated onto a rigid interdigital electrode for comparison with the gas-sensing properties of the MF/ZnS composite.

Characterization

The morphology of the samples was characterized by field-emission scanning electron microscopy (FE-SEM; S-4800; Hitachi, Japan) and optical microscopy (BX53M; Japan). The structure and composition of the samples were characterized by x-ray diffraction (XRD; Bruker D8 Advance, with Cu-Kα radiation) and UV spectrophotometry (UV-Vis; Lambda 650; USA).

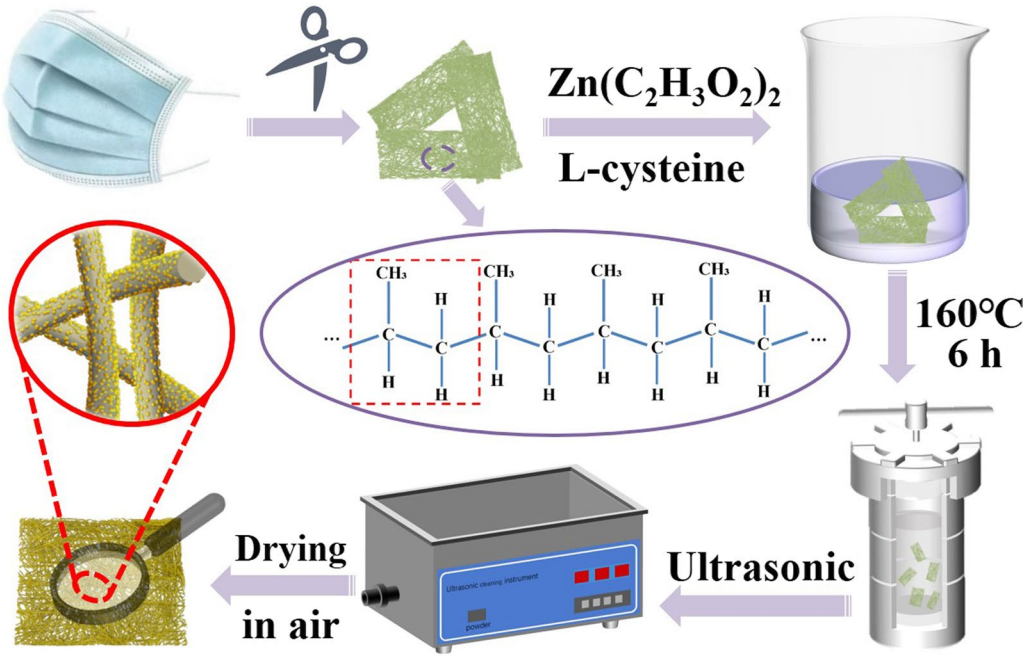

Fig. 1 Flow chart of processing and preparation of MF/ZnS composites.

Results and Discussion

Structure and Morphology Analysis

As can be seen in Fig. 2a, b, the surface of pure MF is smooth and the fiber diameter is about 25.8 μm (inset in Fig. 2a). Although the diameter of the MF/ZnS fibers does not change (inset in Fig. 2c), the fiber surface of MF/ZnS becomes rough due to the loading of ZnS nanoparticles (Fig. 2c–f). The uniform growth of the sensing material layer provides a good foundation for the gas sensitivity and mechanical properties of the MF/ZnS composite.[35] Meanwhile, the surface of the MF/ZnS fibers was etched into spotty pits at high temperatures (inset in Fig. 2e), which facilitated the solid loading of the ZnS nanoparticles. Elemental analysis showed that the MF/ZnS composite contained S and Zn elements in addition to C and O elements (Fig. 2g). The uniform mapping of these S and Zn elements also indicated that the ZnS nanoparticles were uniformly distributed on the surface of the MF. Figure 2h–j shows that the ZnS nanoparticles coated on the rigid substrate exhibited an agglomeration phenomenon due to their large surface energy. Nevertheless, the agglomeration reduces the chance of contact between the ZnS particles and the target gas, which is not conducive to the improvement of the gas-sensing performance of the ZnS particles. For the MF/ZnS composites, the uniform growth of the ZnS particles and the large amount of space between the fibers improved the exposure rate of the sensing material, and enhanced the interaction between the target gas and the sensing material, laying a good foundation for improving the gas-sensing performance.[15,27]

As shown in Fig. 3a, b, compared with pure MF, the MF/ZnS composite still maintains a good fiber structure, and the diameter of the fibers does not change, which is consistent with the observation of SEM. More importantly, it can be seen from Fig. 3a, b that both the pure MF film and the MF/ZnS composite have good gas permeability. As shown by Fig. 3c, the MF/ZnS film is still free of cracks or fractures after 20 g of weight, indicating that the MF/ZnS film has good mechanical strength.[27] As shown in Fig. 3d, the UV-Vis absorption of the MF/ZnS film is stronger than the pure MF, especially in the UV region and the color of the MF/ZnS film becomes darker (Fig. 3d). This suggests that the MF/ZnS film might be used to make UV-shielding clothing. As can be seen from Fig. 3e, the pure MF has two strong diffraction peaks at 14.1° and 17.1°, and two weak diffraction peaks at 18.5° and 21.8°, respectively, which corresponds to the standard card (PDF#54-1936) for PP. The MF/ZnS film not only has the characteristic peaks of PP but also has new diffraction peaks at 28.5°, 47.5°, and 56.3° [36], corresponding to ZnS nanoparticles (PDF#77-2100). The characteristic peaks of the PP of the MF/ZnS composite indicate that the structure of the PP is not destroyed by hydrothermal reaction. This may be the reason why the MF/ZnS composites still maintain good mechanical strength after the hydrothermal reaction.

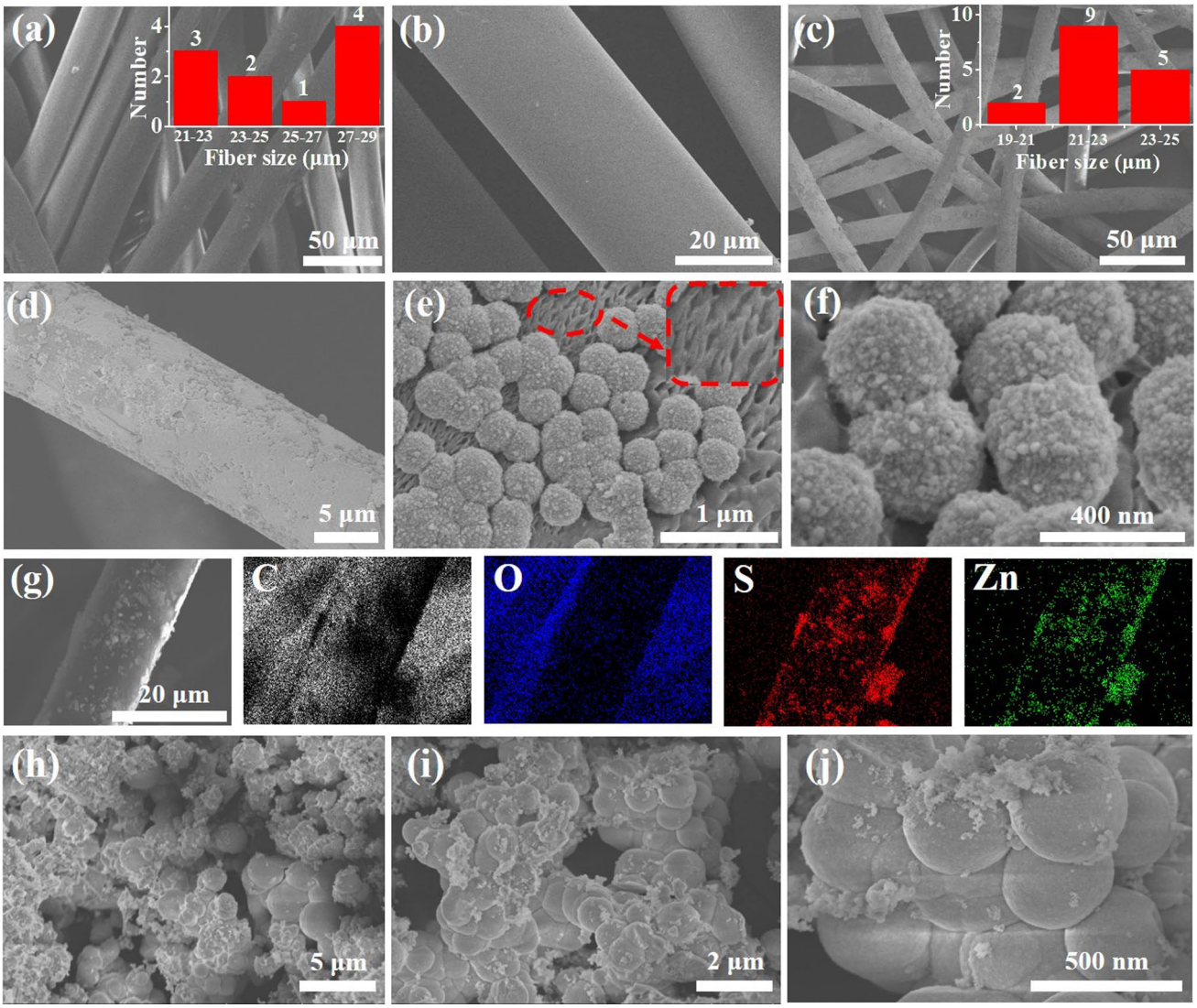

Fig. 2 SEM images of (a, b) pure MF (*inset* in a: statistical diameter of MF), (c–f) MF/ZnS composite (inset in c: statistical diameter of MF/ZnS); (g) element mapping of MF/ZnS composite; (h—j) SEM images of pure ZnS particles.

Gas-Sensing Property of MF/ZnS Composites

The gas-sensitive properties of MF/ZnS films and ZnS powders loaded on ceramic substrates were tested at 4 V using a CGS-MT Multi-functional Probe Station at room temperature and with a relative humidity (RH) of about 35%. The experimental results are shown in Fig. 4a, b for the gas-sensitive properties, and the average response (Fig. 4c) and response time (Fig. 4d) of the ZnS powder and MF/ZnS composite materials, respectively. Both the MF/ZnS film and the ZnS powder loaded on a ceramic substrate showed good stability in three continuous response–recovery cycles. Compared with the ZnS powder loaded on a ceramic substrate, the responses of the MF/ZnS composite to 85% RH and 1000 ppm of NH_3, CH_2O, H_2O_2 have been improved by 35.2 times, 16.2 times, 8.4 times, and 25.1 times, respectively. This is mainly because the MF as the sensing substrate has high gas permeability, which makes the ZnS particles loaded on the MF more fully exposed to contact with the target gas. At the same time, it can be seen that the response of the MF/ZnS sensor to H_2O_2 is more than 16 times that of other gases at the same concentration, showing the good selectivity for H_2O_2. For the MF/ZnS film and ZnS powder loaded on ceramic substrates, their recovery times (Fig. 4e) and response times (Fig. 4a, b) are not more than 3 s and 0 s, respectively, basically showing a fast response. Overall, the response time of the MF/ZnS film to the target analyte is slightly longer than that of the ZnS powder, and its recovery time is shorter than that of the ZnS powder (Fig. 4d, e). Both of them can complete a response–recovery cycle in 30 s. The

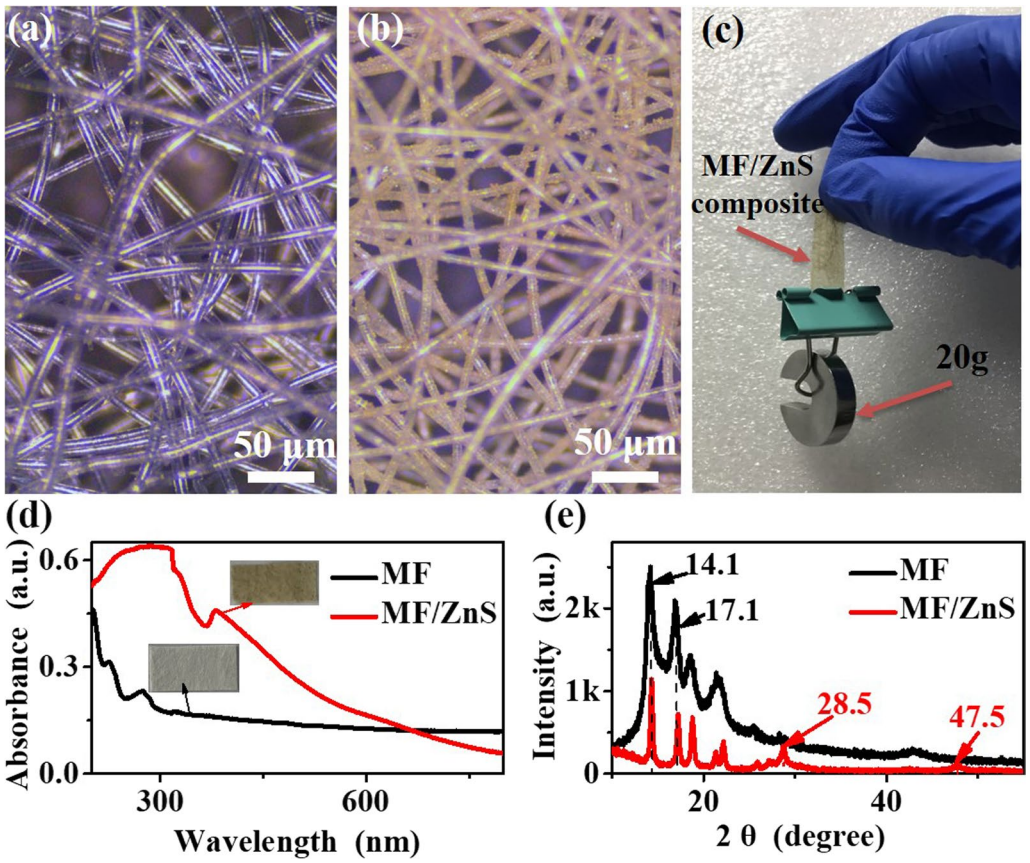

Fig. 3 Optical microscope images of (a) pure MF and (b) MF/ZnS composite; (c) tensile test of MF/ZnS composite; (d) UV-vis absorption spectra; (e) XRD patterns of samples.

good sensing performance of the MF/ZnS film shows that the resource utilization of MF not only reduces the environmental pollution caused by plastic waste and the production cost of sensors but also improves sensing performance.

To verify the generality of this study, several comparative experiments were carried out. ZnS nanomaterials were loaded onto another PP-based mask product disinfected with alcohol (MF-1), new mask products without disinfection (MF-2), and cigarette filter filler (CF) under the same experimental conditions. MF-1/ZnS, MF-2/ZnS, and CF/ZnS were prepared into gas sensors. It can be seen from the XRD patterns (Figure S1) that the positions of the characteristic peaks of the MF-1/ZnS and MF-2/ZnS composites are the same as the MF/ZnS composites. CF is composed of cellulose acetate,[37–40] and the characteristic peak of the pure CF and CF/ZnS in Figure S1 can be seen at 12.7°,[40] while the XRD peaks of ZnS can be seen at 28.5° and 47.5° in the CF/ZnS composite, which indicates that CF/ZnS composites have also been successfully prepared.

The sensing performance of the MF-1/ZnS, MF-2/ZnS, and CF/ZnS composites were tested (Figure S2) and compared with the previous experimental results (Fig. 4). In general, the sensing results of the MF-1/ZnS and MF-2/ZnS sensors are very close, which reflects that the influence of alcohol disinfection on its gas-sensing performance can be basically ignored. Moreover, the MF-1/ZnS and MF-2/ZnS sensors are similar to the CF/ZnS sensor, showing similar sensing trends to the target analytes. In addition, compared with the MF/ZnS, MF-1/ZnS, and MF-2/ZnS sensors, the responses of the CF/ZnS sensor to the target gas has significantly decreased. This may be that the CF of cigarettes does not have as good gas permeability as MF and MF-1, so the gas-sensing performance has also decreased. Nevertheless, their gas-sensing performance is also significantly better than that of ZnS coated on rigid substrates. This shows that our method of using MF to prepare gas sensors has good universality, and that the MF with excellent gas permeability is very suitable for the substrate of gas sensors.

Analysis of Sensing Mechanism

The conductivity of the sensing material depends on the adsorbed gas molecules.[41] It is well known that ZnS is an *n*-type semiconductor.[26] When the MF/ZnS sensor is exposed to reducing gases, such as NH_3 and CH_2O, the gas molecules release electrons into the MF/ZnS in the reaction

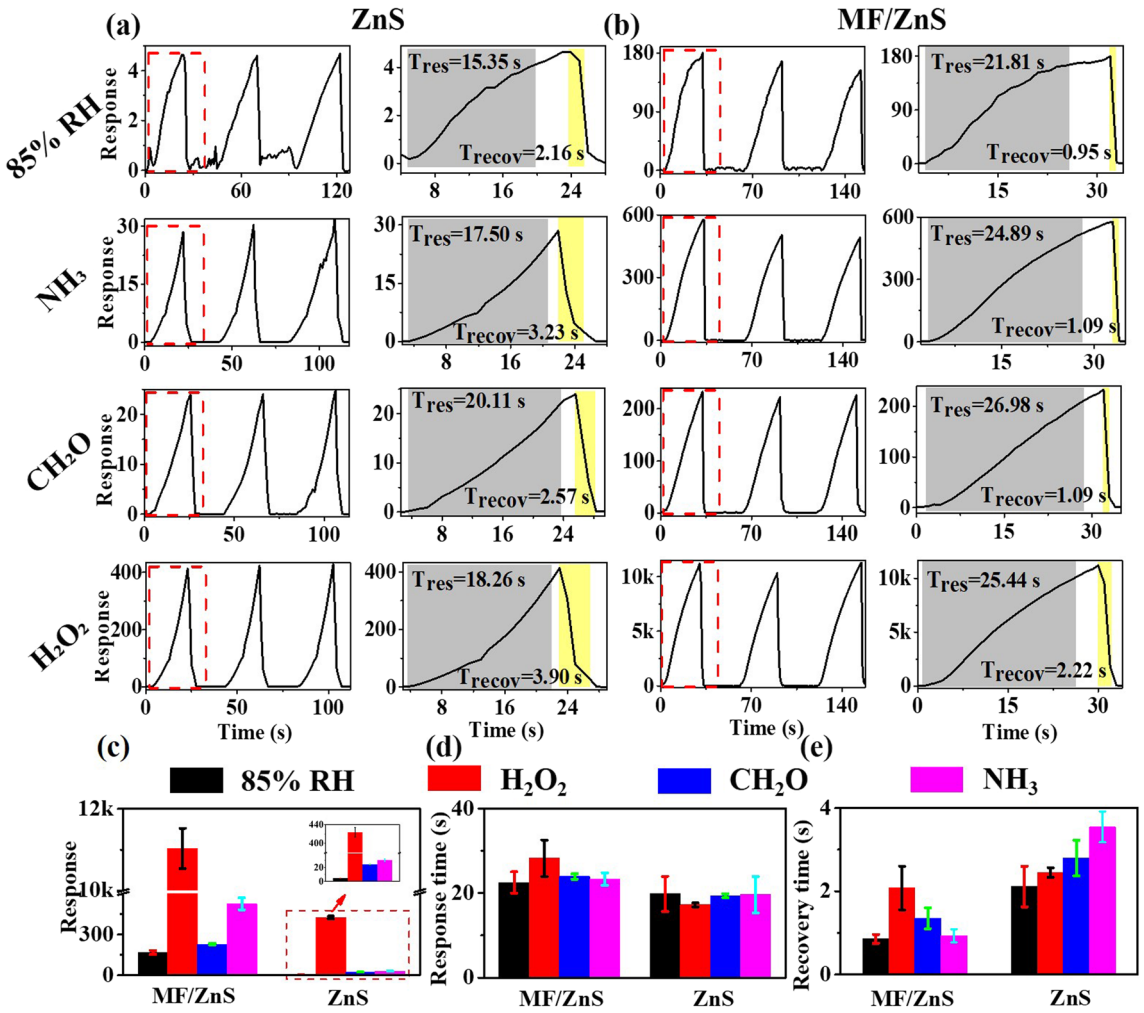

Fig. 4 Sensing curves to different target gases of (a) ZnS loaded on a ceramic substrate, (b) MF/ZnS composite; (c) responses, (d) response times, and (e) recovery time of ZnS and MF/ZnS composite.

process, making the current of MF/ZnS increase rapidly. H_2O_2 is an oxidizing gas; however, the sensing signal of MF/ZnS to H_2O_2 gas is abnormal, which is in the same direction as that of the reducing gas. H_2O_2 is reported to react in the two ways, depending on the concentration of H_2O_2. At high H_2O_2 concentrations (about 10% by volume), the mechanism is[42,43]:

$$2\,H_2O_2 \rightarrow 2\,H_2O + O_2 \quad (1)$$

At a lower concentration (2.1% by volume), the reaction is:

$$2\,H_2O_2 \rightarrow 2\,H_2O + 0.87\,O_2 + 0.08\,O_3 \quad (2)$$

In this work, 30 wt% H_2O_2 was used to produce the H_2O_2 gas by thermal evaporation. According to Eq. (1), the main decomposition products of H_2O_2 are H_2O and O_2. O_2 may be first adsorbed to the surface of the MF/ZnS in the sensing process, and O_2 captures electrons from the MF/ZnS, increasing the charge depletion layer (Fig. 5). The increase of the charge depletion layer will effectively improve the sensitivity of the MF/ZnS sensor. Then, the H_2O vapor is adsorbed on the surface of the MF/ZnS to form a more obvious sensing signal, which is a unique signal belonging to H_2O_2. As a result, the MF/ZnS sensor has a higher sensitivity to H_2O_2, and the sensing signal to H_2O_2 is in the same direction as that at 85% RH.

Conclusions

A MF/ZnS sensor has been prepared for the first time by a hydrothermal method with MF as the sensing substrate. The MF/ZnS sensor showed high sensitivity and recoverability to four analytes at room temperature. Compared with ZnS powder loaded on a ceramic substrate, the MF/ZnS

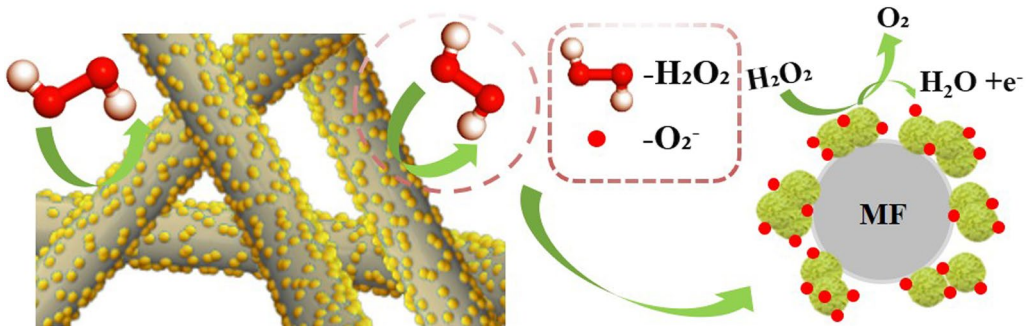

Fig. 5 Possible sensing mechanism of MF/ZnS composites

composite responses to four analytes have been improved by 8.4~35.2 times. This high sensitivity should be contributed to the high permeability of the MF, which makes the ZnS particles loaded on the MF more fully exposed to contact with the target gas. Furthermore, the response of the MF/ZnS composite to H_2O_2 is more than 16 times that of other gases at the same atmospheric concentration, showing high selectivity to H_2O_2. This work provides a new way for the resource utilization of MF and the development of high-performance sensors, inspiring other applications, such as photocatalysis, energy storage, electromagnetic shielding, etc.

Supplementary Information The online version contains supplementary material available at https://doi.org/10.1007/s11664-022-09644-1.

Acknowledgments This research was funded by the Natural Science Foundation of Xinjiang Uygur Autonomous Region (2019D01C019, XJEDU2020Y004), National Natural Science Foundation of China (21964016, 11664038, 61864011), and the Tianshan Innovation Team Program of Xinjiang Uygur Autonomous Region (2020D14038).

Conflict of interest The authors declare that they have no conflicting financial interests or personal relationships that could have appeared to influence the work reported in this paper.

References

1. L. Peeples, What the Data Say About Wearing Face Masks. *Nature* 586, 186–189 (2020).
2. W. He, Y. Guo, H. Gao, J. Liu, Y. Yue, and J. Wang, Evaluation of Regeneration Processes for Filtering Facepiece Respirators in Terms of the Bacteria Inactivation Efficiency and Influences on Filtration Performance. *ACS Nano* 14, 13161–13171 (2020).
3. B.S. Brown, J. Mills, and J.M. Hulse, Chemical and Biological Degradation of Waste Plastics. *Nature* 250, 161–163 (1974).
4. X. Sun, X. Yuan, Y. Jia, L. Feng, F. Zhu, S. Dong, J. Liu, X. Kong, H. Tian, J. Duan, Z. Ding, S. Wang, and B. Xing, Differentially Charged Nano Plastics Demonstrate Distinct Accumulation in Arabidopsis Thaliana. *Nat. Nanotechnol.* 15, 755–760 (2020).
5. P.K. Prajapati, A.M. Kansara, and P.S. Singh, Preparation and Characterization of an Oxygen Permselective Polydimethylsiloxane Hollow Fiber Membrane. *RSC Adv.* 6, 88943–88953 (2016).
6. S.W. Rhee, Management of Used Personal Protective Equipment and Wastes Related to Covid-19 in South Korea. *Waste Manag. Res.* 8, 38 (2020).
7. A. Aragaw, Surgical Face Masks as a Potential Source for Microplastic Pollution in the Covid-19 Scenario. *Mar. Pollut. Bull.* 159, 111517 (2020).
8. A.M. Kansara, S.G. Chaudhri, and P.S. Singh, A Facile One-Step Preparation Method of Recyclable Superhydrophobic Polypropylene Membrane for Oil-Water Separation. *RSC Adv.* 6, 61129–61136 (2016).
9. S. Kim, X. Yang, K. Yang, H. Guo, M. Cho, Y.J. Kim, and Y. Lee, Recycling Respirator Masks to a High-Value Product: From COVID-19 Prevention to Highly Efficient Battery Separator. *Chem. Eng. J.* 430, 132723 (2022).
10. L. Shao, Z. Wu, H. Duan, and T. Shaymurat, Discriminative and Rapid Detection of Ozone Realized by Sensor Array of Zn^{2+} Doping Tailored MoS_2 Ultrathin Nanosheets. *Sens. Actuat. B* 258, 937–946 (2018).
11. D. Miorandi, S. Sicari, F.D. Pellegrini, and I. Chlamtac, Internet of Things: Vision, Applications, and Research Challenges. *Ad. Hoc. Netw.* 10, 1497–1516 (2012).
12. H. Yuan, S.A.A.A. Aljneibi, J. Yuan, Y. Wang, H. Liu, J. Fang, C. Tang, X. Yan, H. Cai, Y. Gu, S.J. Pennycook, J. Tao, and D. Zhao, Biosensors: ZnO Nanosheets Abundant in Oxygen Vacancies Derived from Metal-Organic Frameworks for Ppb-Level Gas Sensing. *Adv. Mater.* 31, 1807161 (2019).
13. D. Zhang, Z. Yang, P. Li, M. Pang, and Q. Xue, Flexible Self-Powered High-Performance Ammonia Sensor Based on Au-Decorated $MoSe_2$ Nanoflowers Driven by Single-Layer $MoSe_2$-Flake Piezoelectric Nanogenerator. *Nano Energy* 65, 103974 (2019).
14. H. Yue, A.M. Soleimanpour, and A.H. Jayatissa, Low Resistive Aluminum-Doped Nanocrystalline Zinc Oxide for Reducing Gas Sensor Application via Sol-Gel Process. *Sens. Actuat. B* 204, 310–318 (2014).
15. H. Liu, M. Li, O. Voznyy, L. Hu, Q. Fu, D. Zhou, Z. Xia, E.H. Sargent, and J. Tang, Physically Flexible, Rapid-Response Gas Sensor Based on Colloidal Quantum Dot Solids. *Adv Mater* 26, 2718–2724 (2014).
16. W. Gao, S. Emaminejad, H.Y.Y. Nyein, K. Chen, A. Peck, H.M. Fahad, H. Ota, H. Shiraki, and D. Kiriya, Fully Integrated Wearable Sensor Arrays for Multiplexed in Situ Perspiration Analysis. *Nature* 529, 509–514 (2016).
17. A. Das, G.R. Kasaliwal, R. Jurk, R. Boldt, D. Fischer, K.W. Stöckelhuber, and G. Heinrich, Rubber Composites Based on Graphene Nanoplatelets, Expanded Graphite, Carbon Nanotubes and Their

Combination: A Comparative Study. *Compos. Sci. Technol.* 72, 1961–1967 (2012).
18. Q. Sun, Z. Wu, Y. Cao, J. Guo, M. Long, and H. Duan, Chemiresistive Sensor Arrays Based on Noncovalently Functionalized Multi-walled Carbon Nanotubes for Ozone Detection. *Sensor Actuat B* 297, 126689 (2019).
19. A. Asghar, A.A. Raman, and W. Daud, Advanced Oxidation Processes for in-Situ Production of Hydrogen Peroxide/Hydroxyl Radical for Textile Wastewater Treatment: A Review. *J. Clean. Prod.* 87, 826–838 (2015).
20. S. Chen, R. Yuan, Y. Chai, and F. Hu, Electrochemical Sensing of Hydrogen Peroxide Using Metal Nanoparticles: A Review. *Microchim. Acta* 180, 15–32 (2013).
21. W. Chen, S. Cai, Q. Ren, W. Wen, and Y. Zhao, Recent Advances in Electrochemical Sensing for Hydrogen Peroxide: A Review. *Analyst* 137, 49–58 (2011).
22. E.I. Muller, C.C. Muller, J.P. Souza, A.L.H. Muller, M.S.P. Enders, M. Doneda, A.C. Frohlich, G.D. Top, and K.F. Anschau, Green Microwave-Assisted Wet Digestion Method of Carbohydrate-Rich Foods with Hydrogen Peroxide using Single Reaction Chamber and Further Elemental Determination Using ICP-OES and ICP-MS. *Microchem. J.* 134, 257–261 (2017).
23. J.M. Rosa, E.B.A. Tambourgi, and J.C.C. Santana, Dyeing of Cotton with Reactive Dyestuffs: the Continuous Reuse of Textile Wastewater Effluent Treated by Ultraviolet/Hydrogen Peroxide Homogeneous Photocatalysis. *J. Clean. Prod.* 90, 60–65 (2015).
24. H. Sakata-Haga, M. Uchishiba, H. Shimada, T. Tsukada, M. Mitani, T. Arikawa, H. Shoji, and T. Hatta, A Rapid and Non-destructive Protocol for Whole-Mount Bone Staining of Small Fish and Xenopus. *Sci. Rep.* 8, 7453 (2018).
25. R. Banavath, R. Srivastava, and P. Bhargava, Nanoporous Cobalt Hexacyanoferrate Nanospheres for Screen-Printed H_2O_2 Sensors. *ACS Appl. Nano Mater.* 4, 5564–5576 (2021).
26. Y.A. Chiao, H. Zhang, M. Sweetwyne, J. Whitson, and P. Rabinovitch, Late-lIfe Restoration of Mitochondrial Function Reverses Cardiac Dysfunction in Old Mice. *Elife* 9, e55513 (2020).
27. W. Zhang, Z. Wu, J. Hu, Y. Cao, J. Guo, M. Long, H. Duan, and D. Jia, Flexible Chemiresistive Sensor of Polyaniline Coated Filter Paper Prepared by Spraying for Fast and Non-contact Detection of Nitroaromatic Explosives. *Sens. Actuat. B* 304, 127233.1-127233.9 (2020).
28. Z. Wu, C. Zhou, B. Zu, Y. Li, and X. Dou, Contactless and Rapid Discrimination of Improvised Explosives realized by Mn^{2+} Doping Tailored ZnS Nanocrystals. *Adv. Funct. Mater.* 26, 4578–4586 (2016).
29. M. Volder, S.H. Tawfick, R.H. Baughman, and A.J. Hart, Carbon Nanotubes: Present and Future Commercial Applications. *Science* 339, 535–539 (2013).
30. M.E. Franke, T.J. Koplin, and U. Simon, Metal and Metal Oxide Nanoparticles in Chemiresistors: Does the Nanoscale Matter? *Small* 2, 36–50 (2010).
31. S. Bai, C. Sun, P. Wan, C. Wang, R. Luo, Y. Li, J. Liu, and X. Sun, Transparent Conducting Films of Hierarchically Nanostructured Polyaniline Networks on Flexible Substrates for High-Performance Gas Sensors. *Small* 11, 306–310 (2015).
32. D. Zhang, C. Jiang, P. Li, and Y. Sun, Layer-by-Layer Self-Assembly of Co_3O_4 Nanorod-Decorated MoS_2 Nanosheet-Based Nanocomposite Toward High-Performance Ammonia Detection. *ACS Appl. Mater. Interfaces* 9, 6462–6471 (2017).
33. W. Zhang, X. Zhang, Z. Wu, K. Abdurahman, and D. Jia, Mechanical, Electromagnetic Shielding and Gas Sensing Properties of Flexible Cotton Fiber/Polyaniline Composites. *Compos. Sci. Technol.* 188, 107966 (2019).
34. C. Fang, D. Cen, Y. Wang, Y. Wu, and G. Han, Zns@ZIF-8 Core-Shell Nanoparticles Incorporated with ICG and TPZ to Enable H_2S-Amplified Synergistic Therapy. *Theranostics* 10, 7671–7682 (2020).
35. W. Zhang, X. Zhang, Z. Wu, K. Abdurahman, and D. Jia, Mechanical, Electromagnetic Shielding and Gas Sensing Properties of Flexible Cotton Fiber/Polyaniline Composites. *Compos. Sci. Technol,* 188, 107966 (2019).
36. D.T. Dova, O. Volobujeva, J. Klauson, A. Mere, and M. Krunks, ZnO Nanorods via Spray Deposition of Solutions Containing Zinc Chloride and Thiocarbamide. *Nanoscale Res. Lett.* 2, 391–396 (2007).
37. R. Zhang, Q. Chen, Z. Zhen, X. Jiang, M. Zhong, and H. Zhu, Cellulose-Templated Graphene Monoliths with Anisotropic Mechanical, Thermal, and Electrical Properties. *ACS Appl. Mater. Int.* 7, 19145–19152 (2015).
38. S. Marinello, F. Lolli, R. Gamberini, and B. Rimini, A Second Life for Cigarette Butts? A Review of Recycling Solutions. *J. Hazard Mater.* 384, 121245 (2019).
39. F. Thuemmler, V. Hettrich, Schmidt, *Properties and Applications of Cellulose Acetate*. Macromol Symposia (2008)
40. R. Li, X. Tian, M. Wei, A.A. Dong, X. Pan, Y. He, and X. Song, Flexible Pressure Sensor Based on Cigarette Filter and Highly Conductive mxene Sheets. *Compos. Commun.* 27, 100889 (2021).
41. J. Li, Y. Liu, J. Zhang, X. Liang, and H. Duan, Density Functional Theory Study of the Adsorption of Hydrogen Atoms on Cu_2X (X=3d) Clusters. *Chem. Phys. Lett.* 651, 137–143 (2016).
42. N. Näther, H. Henkel, A. Schneider, and M.J. Schöning, Investigation of Different Catalytically Active and Passive Materials for Realising a Hydrogen Peroxide Gas Sensor. *Phys. Status. Solid.* 206, 449–454 (2010).
43. E. Capua, R. Cao, C.N. Sukenik, and R. Naaman, Detection of Triacetone Triperoxide (TATP) with an Array of Sensors Based on Non-specific Interactions-ScienceDirect. *Sens. Actuat. B* 140, 122–127 (2009).